Effect of Aging Treatments on the Repassivation Potential of Duplex Stainless Steel S32205

N. Sridhar,[‡,] G. Tormoen,[**] S. Hackney,[***] and A. Anderko[****]*

ABSTRACT

The effect of isothermal heat treatments at 475, 700, and 870°C on the localized corrosion susceptibility of 2205 duplex stainless steel (UNS S32205) was assessed in chloride-containing environments at 60°C. Microstructural changes with heat treatment were analyzed with scanning transmission electron microscopy (STEM) for thermally treated S32205. The results of the tests indicate that exposure of S32205 to these temperatures resulted in an initial drop in the crevice repassivation potential (E_{rcrev}). This drop was partially recovered for specimens aged at 870°C for times longer than 5 h, but the recovery was not observed for the 700°C aged material. The drop in E_{rcrev} correlated with the precipitation and growth of Cr-depleted secondary austenite as well as a grain boundary chromium-depleted (GBCD) layer between a Cr-rich precipitate and the decomposing ferrite matrix. The depletion severity of the secondary austenite phase differed for S32205 aged at 700°C and 870°C, with the 700°C aged materials yielding a secondary austenite phase containing approximately 12.5% Cr and the 870°C precipitated secondary austenite containing approximately 15.8% Cr. The formation of secondary austenite results in a non-recoverable loss of localized corrosion resistance for S32205.

KEY WORDS: aging, duplex stainless steel, model, sensitization, sigma

Submitted for publication March 2009; in revised form, May 2009.

‡ Corresponding author. E-mail: narasi.sridhar@dnv.com.
* Det Norske Veritas, 5777 Frantz Road, Dublin, OH 43017.
** Southwest Research Institute, Department of Materials Engineering, 6220 Culebra Road, San Antonio, TX 78238.
*** Department of Materials Science, Michigan Technological University, 1400 Townsend Drive, Houghton, MI 49931.
**** OLI Systems Inc., 108 American Road, Morris Plains, NJ 07950.

INTRODUCTION

Duplex stainless steels, containing approximately equal volume percents of austenite and ferrite, are used in many applications because of the attractive combinations of strength, corrosion resistance, and stress corrosion cracking resistance. The volume fractions of austenite and ferrite are controlled by alloying additions (C, Mn, Ni, and N stabilize the austenite phase and Cr, Mo, and W stabilize the ferrite phase) in combination with post-solidification thermomechanical processing. In addition to their effect on phase stability, the Cr, Mo, W, and N content of the stainless steel also increase the localized corrosion resistance. Because these attractive properties depend on achieving an appropriate distribution and chemistry of austenite and ferrite, any fabrication process that results in phase transformation can have deleterious consequences on the mechanical properties and corrosion resistance. The richness of the metallurgical reactions, their effects on alloying element redistribution within the microstructure, and the consequent changes in corrosion resistance have prompted much research into these alloys. The phase transformations of interest to corrosion resistance of duplex stainless steels can be divided roughly into two temperature regimes:

—transformations occurring following complete or partial ferritizing depending on the alloy (above approximately 1,300°C), including reactions that occur through postferritizing annealing at lower temperatures[1-3]

ISSN 0010-9312 (print), 1938-159X (online)
09/000119/$5.00+$0.50/0

—transformations that occur due to prolonged exposure to aging temperatures below about 1,000°C

The high-temperature partial ferritization of a nitrogen-containing duplex stainless steel results in the supersaturation of the ferrite with nitrogen that, upon cooling, results in nitride precipitates of the M_2N type and primary austenite (referred to here as γ_1). The "M" in the M_2N precipitates is predominantly chromium, but the duplex stainless steels containing Mo and W may also contain high levels of these alloying elements.[2] Upon reheating this ferritized and quenched structure, a secondary austenite (γ_2) forms through a cooperative precipitation mechanism with M_2N.[2] The secondary austenite is low in alloying elements, such as Cr, Mo, and W, rendering it susceptible to corrosion. In weld fabrication of these alloys, the weld filler metal composition is designed to produce a roughly equal volume fraction of austenite and ferrite such that the weld metal itself retains the properties of the base metal. However, the heat-affected zone adjacent to the weld can see high-temperature exposure that results in partial ferritizing and nitride precipitation. There have also been cases of autogenous welding where the weld zone underwent deleterious high-temperature nitride precipitation.[4] However, the focus of the present paper is on the effects of aging at temperatures below 1,000°C.

The transformations that occur during the aging of duplex stainless steels below their typical mill-annealing temperatures (ranging from 1,038°C to 1,050°C) have been the subject of much study because of the deleterious effect of intermetallic phases and carbides on the mechanical properties and corrosion resistance.[5-18] These studies have shown that:

—in the temperature range from 900°C to 600°C, the formation of χ, σ, $M_{23}C_6$-type carbide, and secondary austenite (γ_2) occurs leading to increased localized corrosion and reduced toughness;

—the increased localized corrosion is manifested by increased intergranular corrosion rate in oxidizing sulfuric acid solutions, higher reactivation kinetics in electrochemical potentiokinetic reactivation tests, decreased critical pitting/crevice temperatures, decreased breakdown potentials, and increased corrosion rates in oxidizing chloride solutions;

—the repassivation potentials in chloride solutions decreased by as much as 1,400 mV upon aging in the 600°C to 900°C range;

—in the temperature range of 475°C, spinodal decomposition and formation of α' regions rich in Cr occurs; and

—in the 475°C regime, the toughness is significantly decreased, but the intergranular corrosion rate increases only moderately in oxidizing sulfuric acid solutions.

—The localized corrosion resistance in terms of breakdown and repassivation potentials decreases only marginally upon exposure to the 475°C range.

Although these studies have clearly demonstrated that the localized corrosion resistance of duplex stainless steels is affected drastically by aging in the 900°C to 600°C temperature regime, such effects were attributed rather vaguely to Cr and Mo depletion due to intermetallic and carbide phase precipitation. However, from our prior studies on Ni-based alloys (Alloys 600 [UNS N06600][1], 825 [UNS N08825], and 22 [UNS N06022]), it was clear that the reduction in repassivation potentials for localized corrosion due to the precipitation of intermetallic or carbide phases in the grain boundaries was rather modest (100 mV to 250 mV) in comparison to that observed for duplex stainless steels.[18-21] These contrasting observations suggest that the spatial extent of depletion of alloying elements in duplex stainless steels must be much greater than in Ni-based alloys.

The main objective of this study was to evaluate the microchemical causes for the drastic reduction in repassivation potential for crevice corrosion observed in duplex stainless steel 2205 (UNS S32205). A further objective of the paper was to model the effect of aging on the repassivation potential using a model formulation that has already been presented.[22-24] In our previous work on modeling repassivation potentials, we have shown that the experimental values of repassivation potential generated for a limited set of environments could be used to predict the values for a much wider set of environments containing aggressive, inhibitive, and diluent species. Thus, the model can be used to compare the experimental results presented in this paper with results generated by others in other environments.

EXPERIMENTAL PROCEDURES

Materials

The compositions of S32205 used in this study are shown in Table 1. The effect of small heat-to-heat variation on corrosion resistance is neglected in presenting the results in this paper. Some specimens were tested in the mill-annealed (as-received) condition, while others were subjected to thermal heat treatments at 475, 700, 870, or 1,250°C for times up to 480 h. Upon reaching the specified thermal heat treatment time, specimens were immediately quenched to room temperature in an agitated water bath.

All specimens meant for corrosion testing were polished on a silicon carbide (SiC) grinding wheel in

[1] UNS numbers are listed in *Metals and Alloys in the Unified Numbering System*, published by the Society of Automotive Engineers (SAE International) and cosponsored by ASTM International.

TABLE 1
Chemical Compositions of the Materials[A]

		wt%							
Alloy	**Lot**	**Fe**	**Ni**	**Cr**	**Mo**	**Mn**	**C**	**N**	**Si**
S32205	AB130	Bal.	5.8	22.5	3.2	1.55	0.017	0.164	0.41
S32205	AB260	Bal.	5.7	22.5	3.22	1.42	0.018	0.172	0.35

[A] Both heats were obtained as plate material.

sequence from 60 grit to 600 grit, and subsequently degreased in a 10-min ultrasonic acetone (CH_3COCH_3) bath. Immersion into test solutions occurred within 1 h of degreasing.

Crevice Repassivation Potential Measurements

Crevice repassivation potential tests were carried out in chloride environments ranging in concentration from 0.4 M Cl^- to 0.04 M Cl^-. Crevice repassivation potential (E_{rcrev}) measurements were recorded from scans made following the potential staircase method. Solutions were prepared by adding 4.69 g or 46.9 g of sodium chloride (NaCl) to 2 L of deionized water (17 MΩ·cm to 18 MΩ·cm) to yield 0.04 M and 0.4 M Cl^- solutions, respectively. Prior to testing, test cells were deaerated by purging with grade 5.0 nitrogen for a minimum of 1 h. Cells were heated to and maintained at 60°C by inserting into a thermostatically controlled heater that continuously monitored the temperature of the test solution.

Potential staircase (PS) scans utilized a protocol that raised the working electrode potential to a specified value (400 mV vs. saturated calomel electrode [SCE] to 500 mV_{SCE}) and held that potential for up to 4 days. A "charge trigger" was implemented during the potentiostatic hold step, which would automatically reverse the potential scan if a charge density of 10°C/cm^2 (31.5 mA·h, assuming uniform distribution over the whole crevice area) was achieved. The potential was then scanned in the reverse direction at a rate of –0.0167 mV/s to a final potential of –400 mV_{SCE}. E_{rcrev} was recorded as the highest potential that corresponded to a current density of <1 μA/cm^2 when scanned in the reverse direction.

Cyclic potentiodynamic polarization (CPP) tests were also conducted on the S32205 alloy, but yielded inconsistent data. The reasons for the failure of CPP tests to yield consistent repassivation potentials even for the same annealing treatment may be related to the tendency of the potentials to attain high values in the transpassive regime. In such cases, true crevice corrosion did not occur, resulting in high values of "repassivation potentials." This issue was addressed in our previous paper.[22] Therefore, CPP results were abandoned from further consideration. The recorded data were confirmed by posttest examination of the specimen for signs of localized corrosion.

† Trade name.

Microscopy

Specimens meant for scanning transmission electron microscopy (STEM) analysis were polished on a 600-grit grinding wheel to approximately 10 mils to 15 mils thick. Next, 3-mm discs were punched from the foil with a 3-mm TEM disc punch. The disks were then polished to sub-10 mil thicknesses on both sides and degreased in an ultrasonic acetone bath. The samples were then electropolished using a 5% perchloric acid ($HClO_4$) + 20% acetic acid ($C_2H_4O_2$) + 75% methanol (CH_3COOH) solution at 0°C. A JEOL 4000 FEX† analytical electron microscope was used in both TEM and STEM modes for imaging, diffraction, and energy-dispersive spectrometry data collection. The k factors for elemental analyses were determined using a mill-annealed sample as a standard in which the ferrite and austenite grain compositions had been measured via the microprobe.

RESULTS

Crevice Repassivation Potentials with Thermal Aging

The results of the PS test method for the as-received duplex S32205 stainless steel in 0.04 M and 0.4 M NaCl solutions are shown in Figures 1 and 2, respectively. It can be seen that at the applied potential of 0.4 V_{SCE}, the anodic current density increases slightly indicating active pit growth within the crevices. Upon lowering the potential, the current density decreases until a potential is reached where negative excursions of current are observed, followed by complete repassivation (inset in figures). It is interesting to note that during the potential reduction scan, the current shows periodic increases, indicating an initial decrease in the dissolution rate followed by an increase toward a higher value as the concentration gradients within the pits stabilize. It is only upon complete repassivation that the current remains at a low value. The PS scan for the 870°C aging treatment is shown in Figure 3. It can be seen that during the downward potential scan, two dips in the current are observed. The first dip in the current at about 0.1 V was somewhat transient and occurred at a relatively high current density, whereas the second dip at about –0.2 V represented a complete repassivation. A similar behavior was observed for the 700°C, 480-h aging treatment (Figure 4). On the other hand, the 700°C,

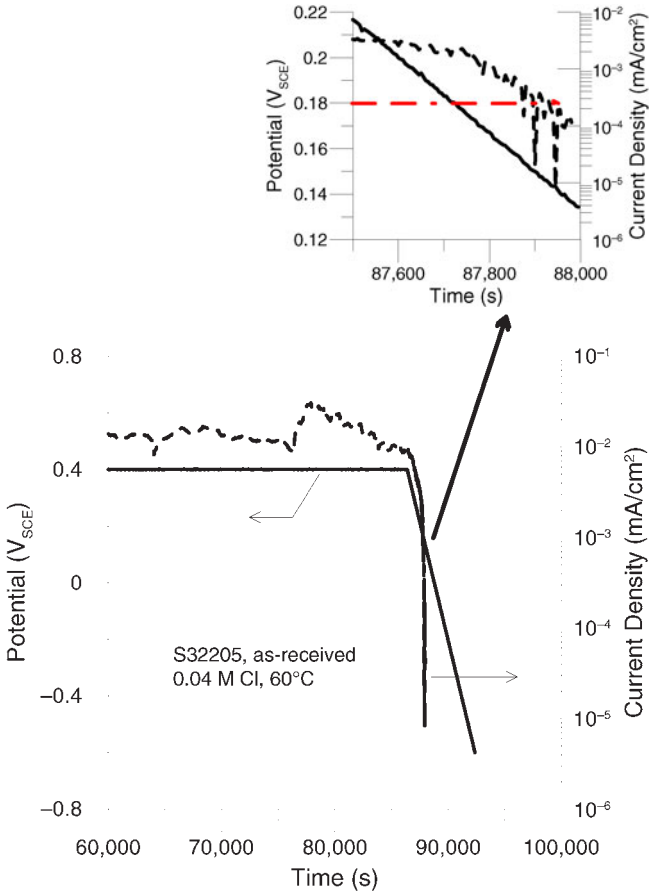

FIGURE 1. *Potential staircase method scan for as-received duplex stainless steel S32205 in 0.04 M NaCl solution at 60°C. The inset figure indicates the detailed region near repassivation.*

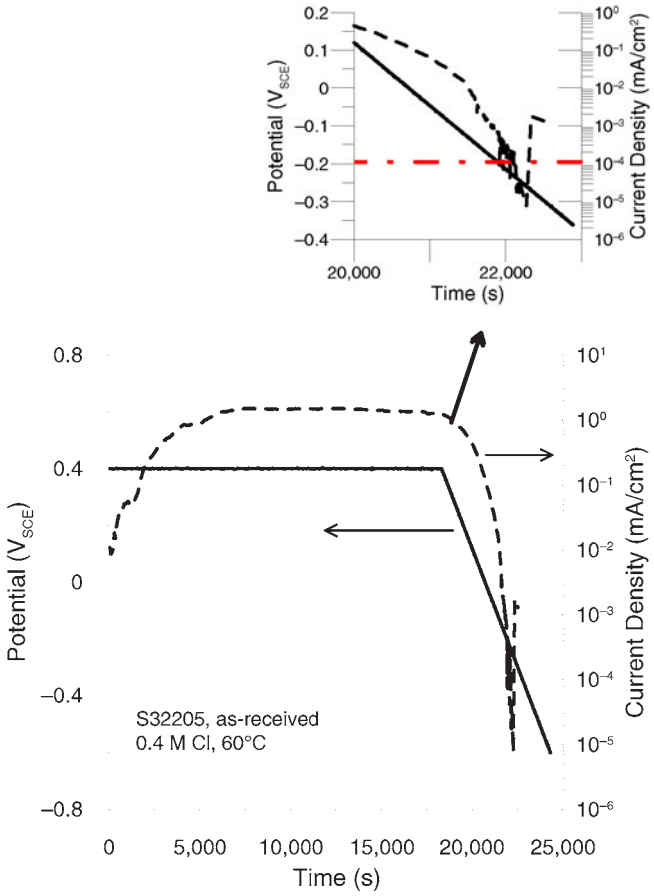

FIGURE 2. *Potential staircase method scan for as-received duplex stainless steel S32205 in 0.4 M NaCl solution at 60°C. The inset figure indicates the detailed region near repassivation.*

24-h and the 475°C, 2-h aging treatments did not show the two-step behavior (Figure 5).

The measured E_{rcrev} values for isothermally heat-treated S32205 in 0.4 M chloride solutions are shown in Figure 6. In the 700°C and 870°C aging conditions, a decrease in repassivation potential was observed at intermediate aging times, whereas at longer times a small recovery of the repassivation potential was observed. The initial increase in repassivation potential from the mill-annealed specimen is unclear and may be related to dispersion in the repassivation potential data. The 475°C aging produced a smaller decrease in repassivation potential, but longer aging treatments were not conducted for this temperature in this study. Similar effects were observed for aged specimens tested in the 0.04-M chloride solution (Figure 7). The effect of chloride concentration on repassivation potential for several thermal treatment conditions is shown in Figure 8. For the 1,250°C treatment, the effect of thermal treatment is observed mainly at lower chloride concentrations.

The corrosion morphology is shown in Figure 9. For the 1,250°C treatment, the corrosion is mainly inside the ferrite grains and along the grain boundaries. For 870°C and 700°C aging, the corrosion appears to be preferential to the ferrite phase and along the sigma-ferrite boundaries. The extent of corrosion is much greater for the 700°C aged sample.

Scanning Transmission Electron Microscopy Analyses

At 700°C, precipitation occurred at both α/γ and α/α boundaries in as little as 0.5 h. A representation of each, along with the energy-dispersive x-ray spectroscopy (EDS) composition profiles that trace the arrow are shown in Figure 10. The composition profiles are shown in terms of the ratio of the alloying element to Fe. The α/α precipitates have a sawtooth morphology, while the α/γ precipitates are more cellular. The α/γ precipitates show heavy Mo enrichment and a slight Cr depletion at the grain boundary. The α/γ precipitates show no Cr depletion and a slight Mo enrichment at the grain boundary in the matrix. At ferrite-ferrite boundaries, the decomposing matrix is depleted in Cr when compared to the mill-annealed condition, which showed a Cr/Fe peak intensity ratio of 0.33 for primary austenite and 0.38 for primary ferrite. Similar depletion has been shown by Park, et al.[17]

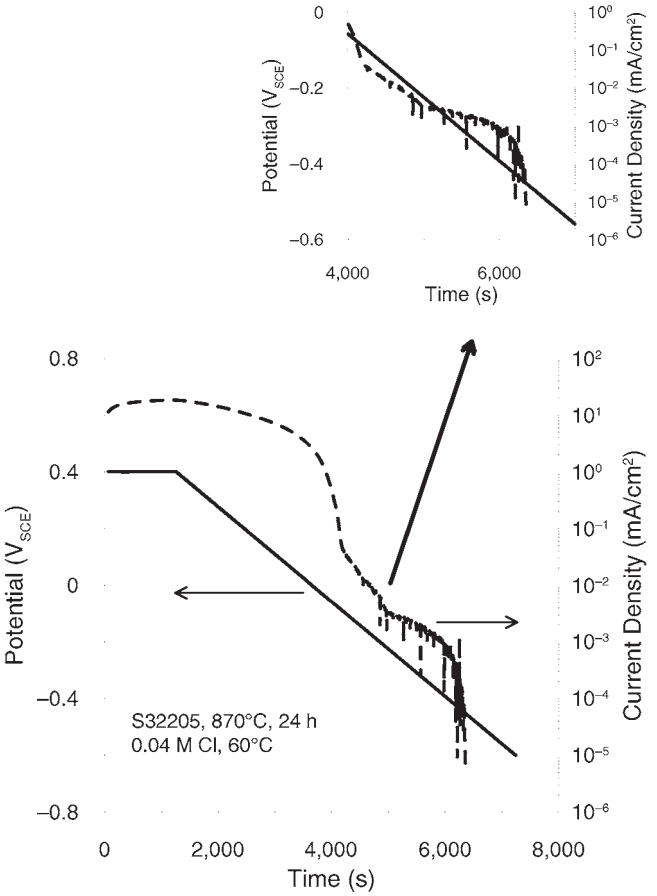

FIGURE 3. *Potential staircase method scan for the duplex stainless steel S32205 aged at 870°C for 24 h, tested in 0.4 M NaCl solution at 60°C. The inset figure indicates the detailed region near repassivation.*

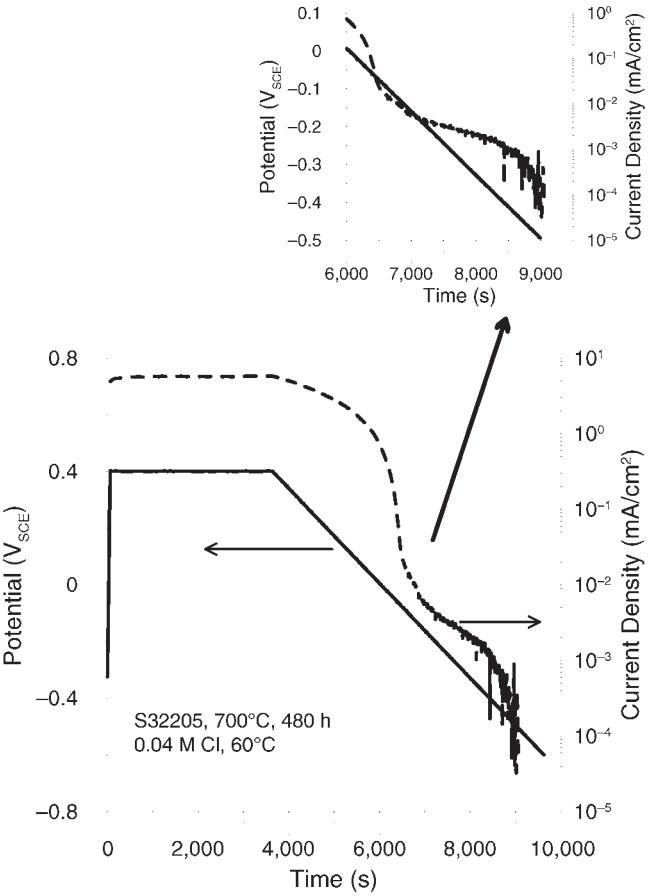

FIGURE 4. *Potential staircase method scan for the duplex stainless steel S32205 aged at 700°C for 48 h, tested in 0.4 M NaCl solution at 60°C. The inset figure indicates the detailed region near repassivation.*

As the heat treatment progressed, increased precipitation was observed. A metallographic image of the precipitated region in the α/α interface after 5 h at 700°C shows that the ferrite has decomposed to a region of Cr-rich precipitates along with a depleted matrix phase (Figure 11). The depleted matrix shows more severe Cr depletion containing approximately half the chromium contained in the mill-annealed ferrite phase. The precipitates at this heat treatment showed slight Cr and Mo enrichment. These phases are likely the eutectoid transformation of $\alpha \rightarrow \sigma + \gamma_2$, a reaction that has been described in the literature.[7-9] In essence, the abstraction of Cr and Mo to the precipitate destabilizes the ferrite phase, which transforms to a secondary austenite phase. Due to its formation mechanism, the secondary austenite is depleted with respect to Cr and Mo as compared to the primary austenite. Outside the precipitated region, the non-transformed ferrite matrix showed some grain-boundary Cr depletion (Figure 12), though the depleted levels were not as severe as those observed in the secondary austenite. This is verified further in Figure 13, which shows the composition profile across a secondary austenite-primary austenite boundary. The transition from the primary phase to the secondary phase is denoted on the profile.

Following 24 h of thermal treatment at 700°C, the lowest E_{rerev} value for S32205 were recorded. STEM imaging revealed that grain boundary chromium depletion (GBCD) was evident for this heat treatment as more heavily etched regions of the TEM specimen during the electropolish step, as illustrated in Figure 14, along with EDS profiles taken from a grain boundary extending into the matrix phase as well as several EDS profiles taken from phases present in the precipitated region. The Cr depletion at the grain boundaries dropped below the Cr level of the secondary austenite (phases marked as 0, 2, 3, and 5). The precipitate at spot 1 shows enormous Cr enrichment, while the precipitate at spot 4 shows little Cr enrichment and only slight Mo enrichment, different from the profiles seen at 0.5 h and 5 h of aging. It is evident that as the isothermal aging time increases, the Cr-depleted secondary austenite continues to grow, constituting an increasing volume fraction of the microstructure. This phase is estimated to contain approximately 12.5% Cr

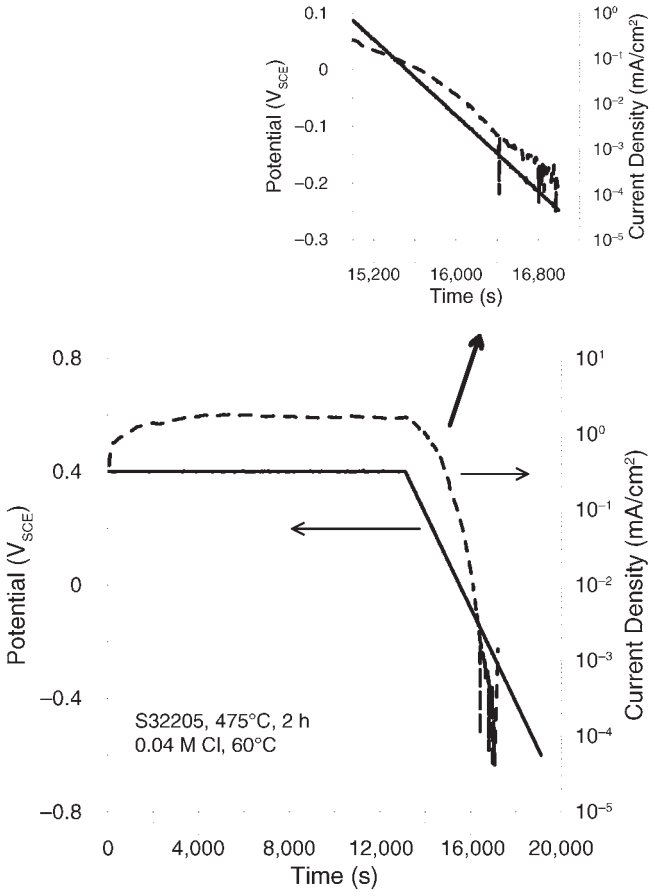

FIGURE 5. *Potential staircase method scan for the duplex stainless steel S32205 aged at 475°C for 2 h, tested in 0.4 M NaCl solution at 60°C. The inset figure indicates the detailed region near repassivation.*

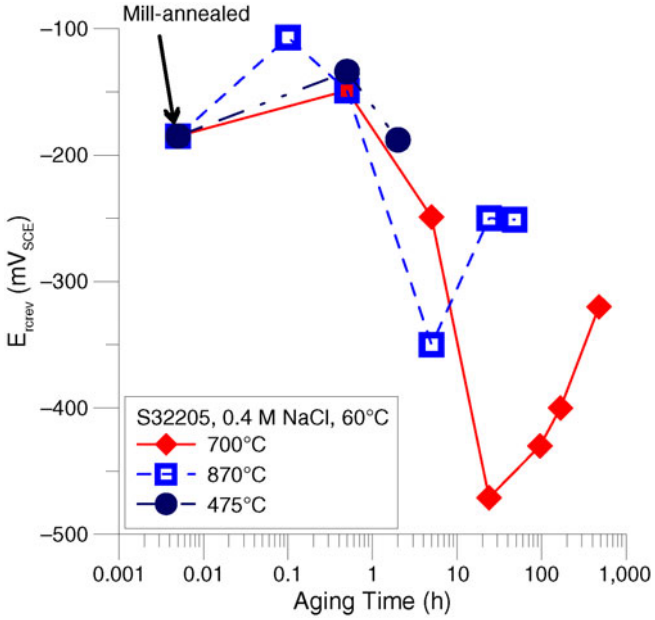

FIGURE 6. *Effect of aging time at three different temperatures on the E_{rcrev} of S32205 in 0.4 M NaCl solution at 60°C.*

based on the Cr/Fe intensity ratios from EDS profiles taken from the secondary austenite and parent ferrite phase from which it precipitated. The primary ferrite is estimated to contain roughly 24% Cr.

STEM imaging was also performed on initial aging times at 870°C. Precipitates appeared larger at this temperature than for comparable treatments at 700°C. Figure 15 shows a precipitated region evident after 0.5 h exposure. The precipitate (a) is shown

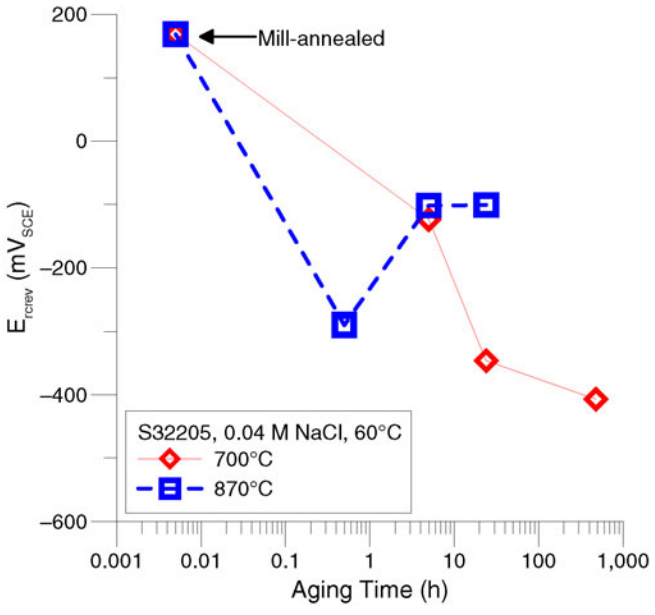

FIGURE 7. *Effect of aging time at two different temperatures on the E_{rcrev} of S32205 in 0.04 M NaCl solution at 60°C.*

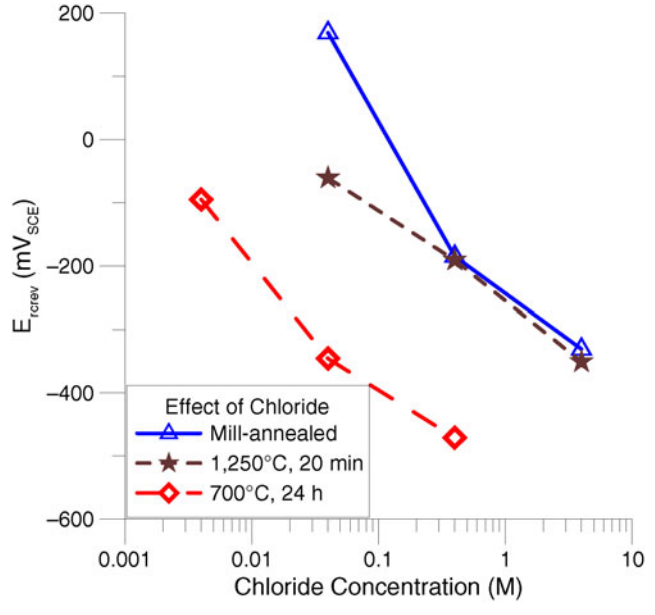

FIGURE 8. *Effect of chloride concentration on the repassivation potential of S32205 for different aging treatments.*

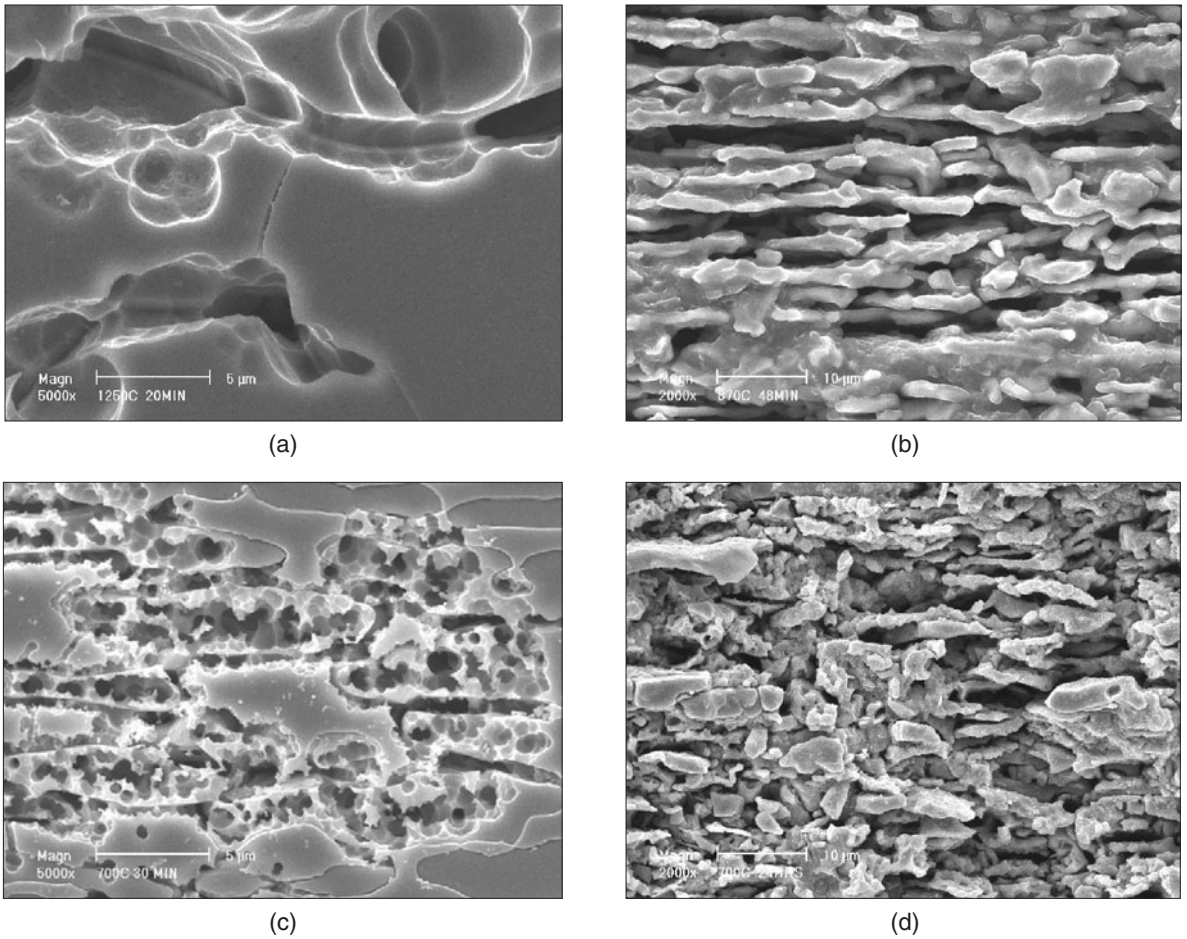

(a) (b)

(c) (d)

FIGURE 9. *Crevice corrosion mode of S32205 after repassivation test. Clockwise from top left: 1,250°C, 20 min; 870°C, 48 min; 700°C, 30 min; and 700°C, 24 h.*

as the dark spike in the image, which is joined by two austenite phases (c and d) that appear to be consuming a ferrite grain (b). The precipitate is highly enriched in Cr, while the two secondary austenite grains are Cr-depleted, though not to the extent seen at 700°C. The intact ferrite grain showed no compositional deviation from the mill-annealed ferrite. However, after 2 h at 870°C, the specimen did not show any ferrite or austenite grains with compositions approaching that observed for the mill-annealed sample. Figure 16 displays the compositions determined at the center of nine different grains, along with a precipitate phase. All of the grains examined were Cr-depleted with respect to the mill-annealed composition. While the Cr-depleted secondary austenite was not as severely depleted as the 700°C aged material, it appeared sooner at 870°C and was more abundant after longer aging times than at 700°C (Figure 14).

DISCUSSION

The decrease in repassivation potential of S32205 in this study is consistent with various observations of the effect of aging on the localized corrosion resistance of duplex stainless steels. For example, Ravindranath and Malhotra[8] found that aging at 700°C reduced the breakdown potential of S32205 by several hundred millivolts and that localized corrosion occurred near austenite phase boundaries. Park, et al.,[17] found a considerable decrease in critical pitting temperature in 6% ferric chloride ($FeCl_3$) solutions upon aging of a 22Cr duplex stainless steel. Amadou, et al.,[11] found that a cast duplex stainless steel showed an almost 1,000-mV decrease in repassivation potential in synthetic seawater when aged in the temperature range between 600°C and 900°C. In their case, the decrease in repassivation potential was much greater than that of the breakdown/pit initiation potential and was relatively independent of the aging temperature. However, they did not measure local composition changes in the alloy.

The decrease in the repassivation potential of the alloy upon aging is dependent on the aging temperature, time, and the test solution. In the 0.4-M chloride solution, longer aging times at both 700°C and 870°C resulted in a partial recovery of the repassivation

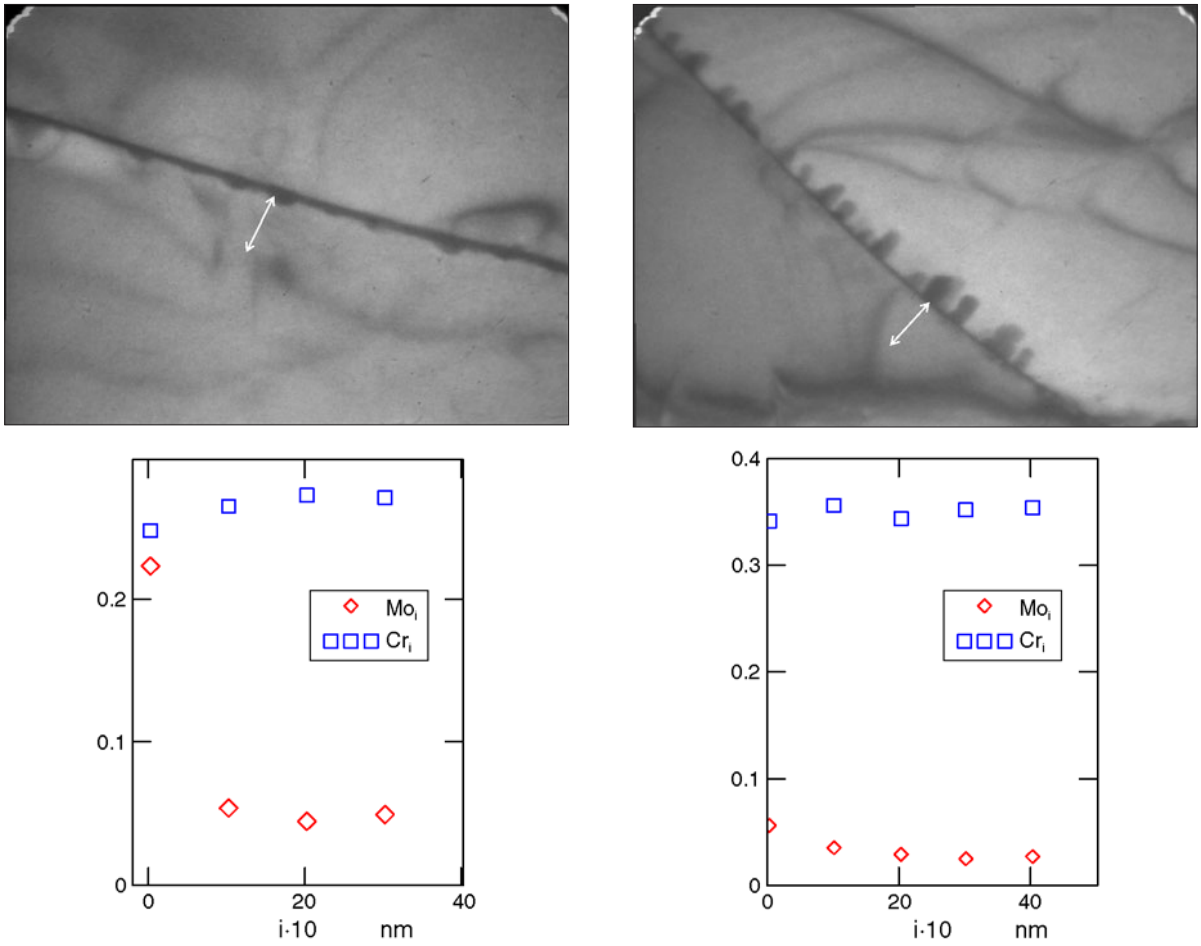

FIGURE 10. *(left) Ferrite-ferrite boundary and (right) ferrite-austenite boundary precipitates observed in S32205 after 0.5 h at 700°C. The ratio of element peak intensities to Fe from EDS are shown on the vertical axes.*

potential. The recovery was more rapid for 870°C than 700°C. For the 0.04-M chloride solution, the 700°C aging did not show a recovery within the aging time periods tested, whereas the 870°C aging showed some recovery. The more rapid recovery at the higher aging temperature may be explained as the result of greater diffusion of the alloying elements into the depleted secondary austenite phase from the ferrite phase. The slower recovery in the 0.04-M chloride solution may be a result of the larger pit size in the lower chloride solution. The pit initiation potential in the 0.04-M chloride solution is higher (more positive) than the pit initiation potential in the 0.4-M chloride solution. This means that when the potential is held at 0.4 V_{SCE} during pit/crevice growth, more pits are likely to nucleate and grow in the 0.4-M chloride solution than in the 0.04-M chloride solution. This would also mean that there will be a smaller number of larger pits in the 0.04-M chloride solution (note that typically all these specimens are held potentiostatically until an average charge density exceeds a preset value). If these larger pits span the secondary austenite grain completely, then the repassivation potential measured in the 0.4-M chloride solution "samples" the whole secondary austenite. Longer aging times may result in some diffusion of Cr and Mo at the edges of the secondary austenite resulting in some recovery. In contrast, pits in the 0.04-M chloride solutions probably nucleate in regions deep inside the secondary austenite where the recovery is slower due to greater diffusion distance from the surrounding ferrite grains.

MODELING OF AGING EFFECTS ON REPASSIVATION POTENTIAL

The experimental results indicate a strong relationship between the measured repassivation potential and the depletion of chromium. This observation raises a question of whether the E_{rp} depression can be predicted quantitatively using the obtained composition profiles. Such a quantitative prediction could be used to confirm the proposed mechanism of E_{rp} depression and would be useful for assessing the localized corrosion resistance of thermally aged duplex alloys in industrial practice.

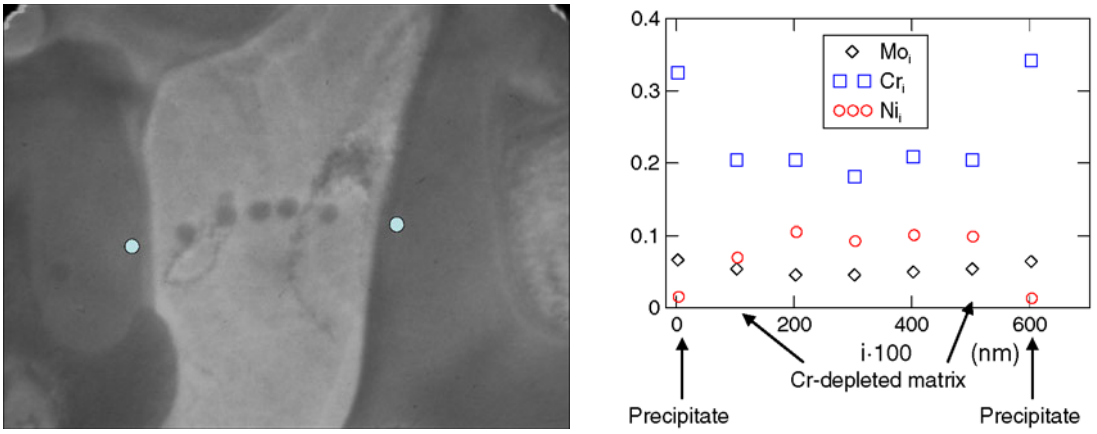

FIGURE 11. *Image of (left) Cr-rich precipitates and secondary austenite along with (right) respective EDS profiles for the dots on the image. Aged 700°C, 0.5 h.*

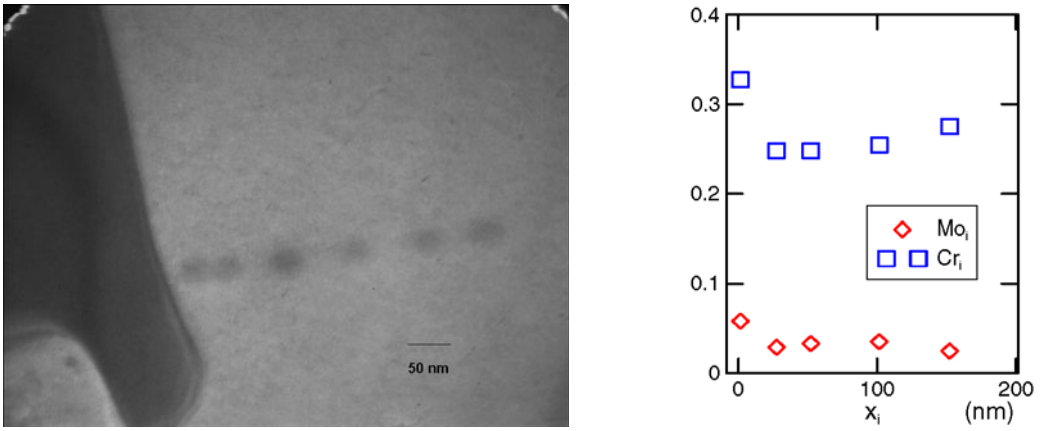

FIGURE 12. *Evidence of GBCD at the precipitate-ferrite interface. Elemental profiles are measured as a function of distance from the precipitate boundary.*

To answer this question, we used a previously developed mechanistic model for calculating the repassivation potential as a function of both alloy composition and solution chemistry of the environment.[22-23] Since the details of this model were described previously,[22-23] only its essential features are summarized here. The model was derived by considering the dissolution of a metal in a localized corrosion environment in the limit of repassivation. The model envisages the dissolution of the metal underneath a layer of a concentrated metal halide solution. In the process of repassivation, a thin layer of oxide is assumed to form at the interface between the metal and the hydrous metal halide. The model represents the formation of the oxide layer using a partial coverage approach. The partial coverage fraction increases as repassivation is approached. The dissolution rate of the metal under the oxide is much lower than at the metal-halide interface and corresponds to the passive dissolution rate. Thus, as the repassivation potential is approached, the dissolution rate tends toward the passive dissolution rate. The model includes the effects of multiple aggressive and nonaggressive or inhibitive species, which are assumed to undergo competitive adsorption. The aggressive species form metal complexes, which dissolve in the active state. The inhibitive species and water contribute to the formation of oxides, which induce passivity. The formalism that describes these phenomena leads to a closed-form equation in the limit of repassivation, i.e., when the current density reaches a predetermined low value, i_{rp} ($i_{rp} = 10^{-2}$ A/m^2), and the fluxes of metal ions become small and comparable to those for passive dissolution. Most importantly for the study of thermally aged alloys, the parameters of the model have been generalized in terms of alloy composition for Fe-Ni-Cr-Mo-W-N alloys.[23] This generalization was based on experimental E_{rp} data for 13 base (typically mill-annealed) stainless steels and nickel-based alloys, supplemented by those for Fe and Ni. The relevant equations and parameters are given by Anderko, et al.[23]

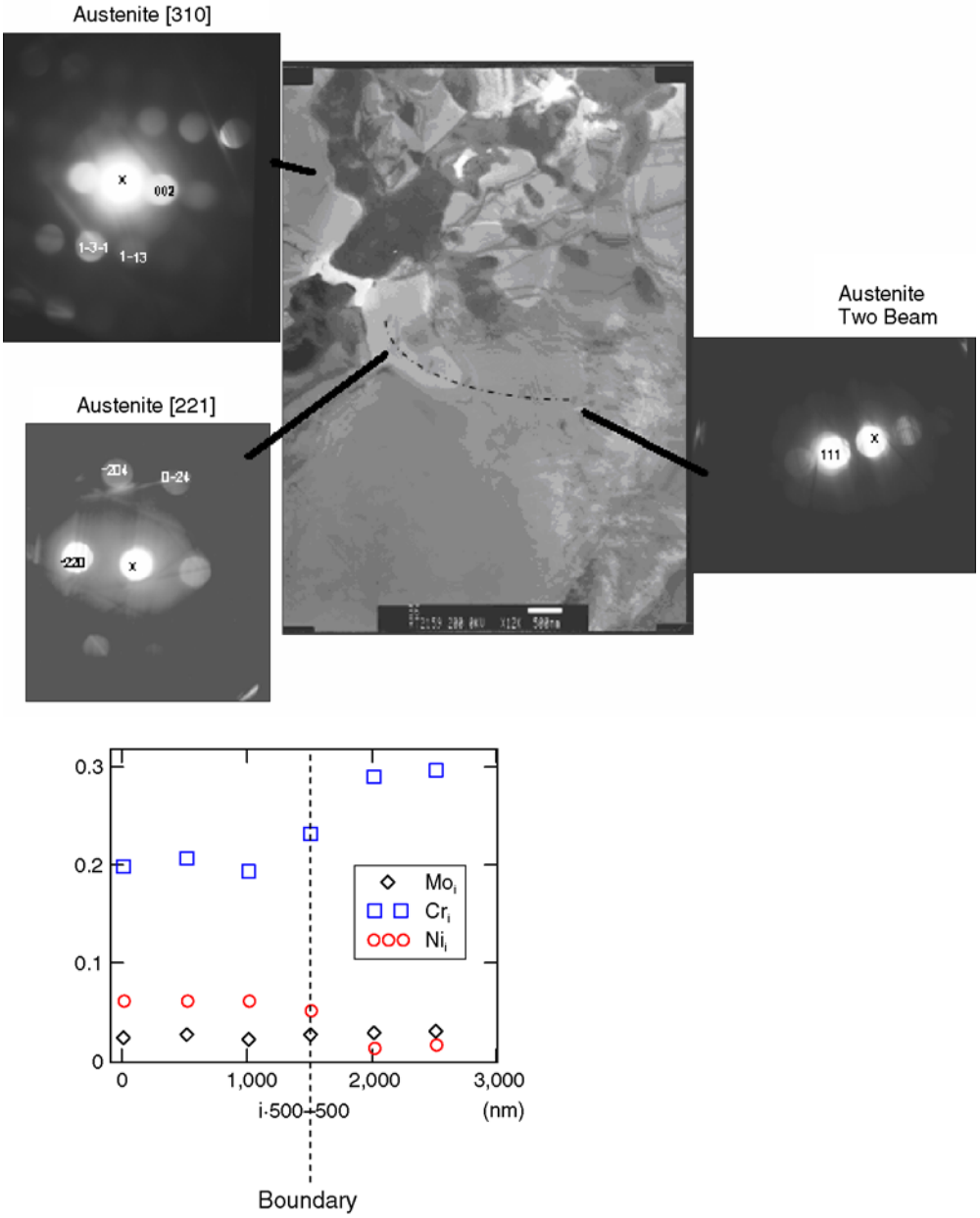

FIGURE 13. *EDS profiles comparing the depleted precipitated matrix phase juxtaposed with the primary matrix phases after 5 h at 700°C. EDS points were taken following the dotted line shown in the micrograph.*

To calculate E_{rp} of thermally aged samples, it is reasonable to assume that the measured E_{rp} primarily reflects the localized corrosion of the regions that are most depleted in chromium. This is due to the fact that a pit stabilizes more easily in an area that is more susceptible to localized corrosion because of chromium (or molybdenum) depletion. In the case of S32205, the lowest-Cr zone corresponds to the secondary austenite phase. Furthermore, as discussed above, the size of the secondary austenite phase is sufficiently large to stabilize a pit. This is important because a certain minimum size is necessary for stabilizing a pit in an E_{rp} measurement. Thus, we can reasonably assume that the repassivation potential of thermally aged S32205 samples can be calculated on the basis of the composition of the secondary austenite phase.

Figure 17 shows the results of calculations using the generalized repassivation potential model[23] for mill-annealed S32205 and for samples heat-treated at 700°C for 5 h and 24 h. To calculate the repassivation potential of the bulk alloy, the composition of lot AB130 (Table 1) was assumed. The composition of lot AA260 would result in essentially the same prediction. The predictions for the bulk alloy are in excellent agreement with the experimental data for mill-annealed S32205 (cf. the thick line and diamonds in Figure 17). To calculate E_{rp} for the 700°C, 5-h sam-

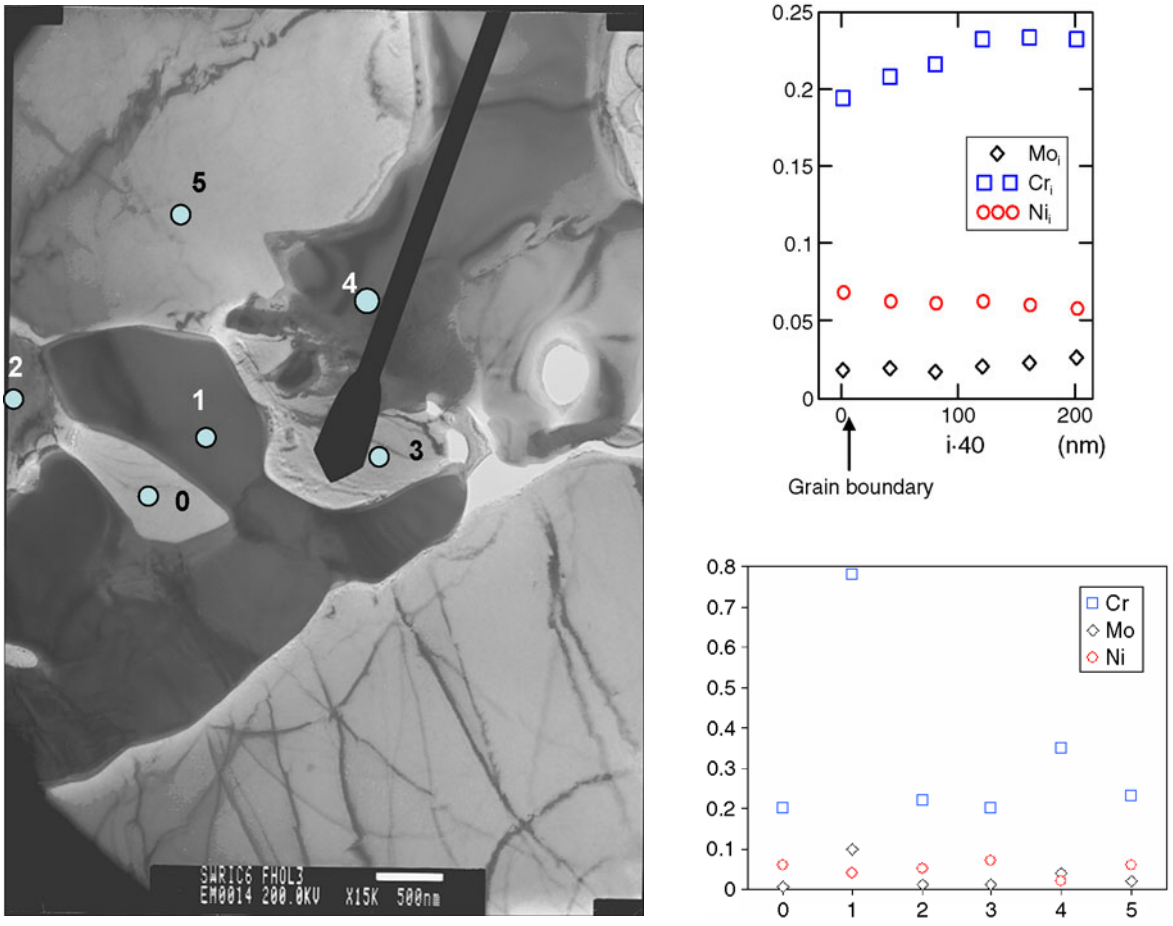

FIGURE 14. *(left) STEM image and (bottom right) corresponding EDS profiles of various phases in the precipitated region of S32205 after 24 h exposure to 700°C. Evidence of sensitization at this heat treatment is evident as preferentially thinned grain boundaries in the image and from the EDS profile taken at the boundary extending into the primary matrix phase. The numbers on the x-axis of the lower right figure (0 through 5) correspond to the numbered locations shown in the TEM micrograph on the left.*

ple, the profiles depicted in Figure 13 were used to estimate the alloy composition (i.e., 14.4% Cr, 3.3% Mo, 5.7% Ni, bal. Fe). For the alloy aged at 700°C and 24 h, the Cr content was assumed to be 12.5% as discussed above and the Mo and Ni content was estimated at 1.4% and 5.1%, respectively (based on the profiles from Figure 14). For both thermally aged samples, it was assumed that the nitrogen content in the secondary austenite remained the same as in the bulk alloy (i.e., 0.164%). This is a reasonable assumption due to the higher diffusivity of nitrogen compared to Cr and Mo. As shown in Figure 17, the calculated E_{rp} values for both thermally aged samples are in reasonable agreement with the data. It should be noted that the predictions are subject to considerable uncertainty because the N content in the secondary austenite phase is unknown and the Mo content is highly uncertain (because of the small Mo intensity ratios). Thus, the predicted repassivation potentials should be considered satisfactory. The calculations indicate that the E_{rp} values measured for the heat-treated samples can be explained quantitatively by the composition of the secondary austenite.

CONCLUSIONS

❖ In this study, localized corrosion susceptibility of S32205 through crevice repassivation potential measurements in chloride solutions was determined as a function of isothermal heat treatment time. It was found that at 700°C, a drop of ~450 mV was observed with initial aging of this material, which only slightly recovered after long aging times. A similar drop was noted at 870°C, but this was partially recovered (by 100 mV) with prolonged isothermal aging.

❖ Microstructural characterization of precipitated phases of S32205 was performed with STEM. Both ferrite-ferrite and ferrite-austenite boundary precipitates were noted for both thermal aging temperatures. At 700°C, a eutectoid-like transformation had occurred where the ferrite decomposed to sigma and secondary austenite. The composition of this sec-

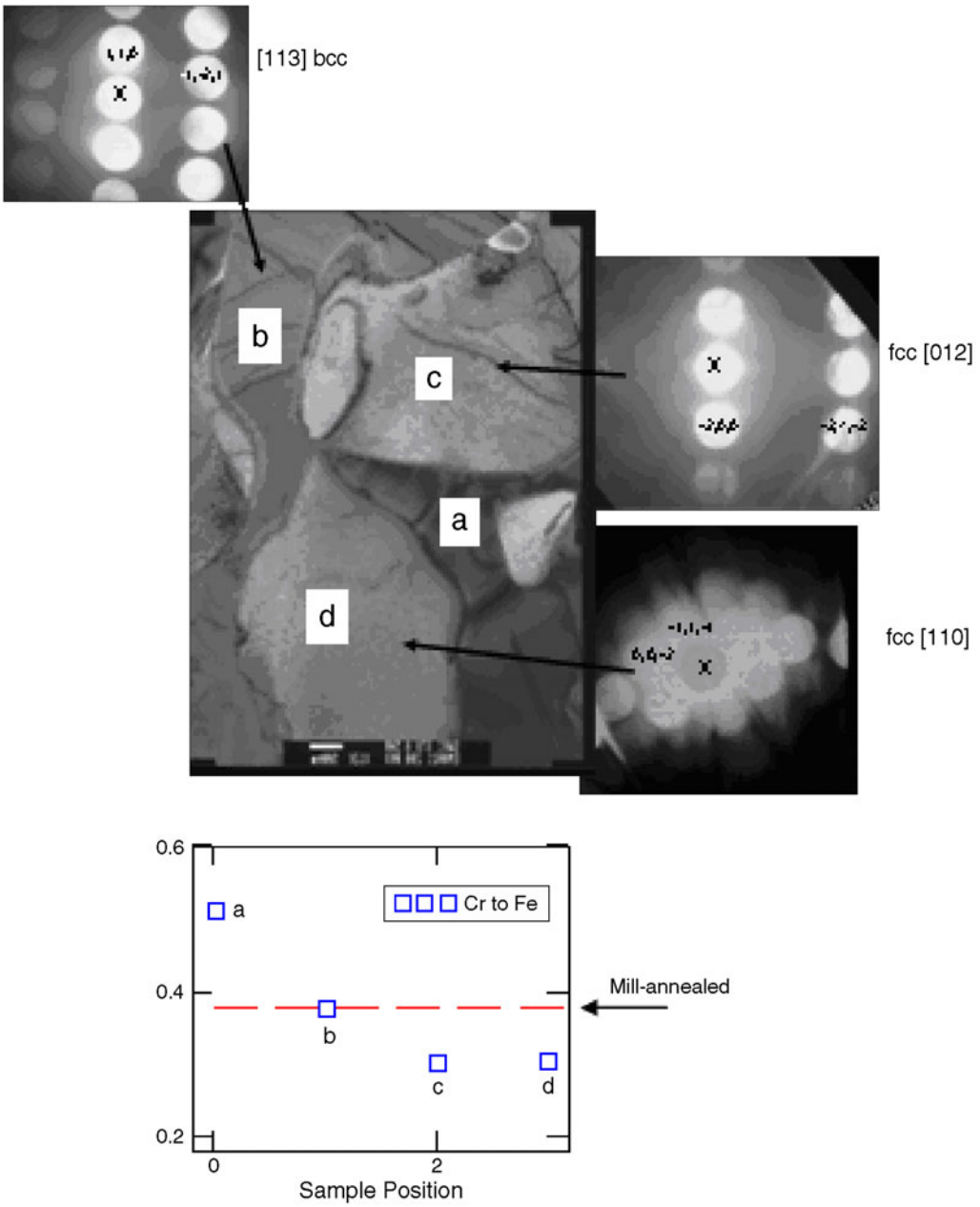

FIGURE 15. *Selected area diffraction (SAD) images of phases evident for S32205 after 0.5 h exposure to 870°C, and corresponding EDS. The labels (a through d) in the bottom figure correspond to the locations indicated in the top figure.*

ondary austenite was found to contain roughly half the chromium of the primary austenite, and caused the isothermally aged material to become susceptible to localized corrosive attack. At 870°C, the precipitates were more globular and pervasive throughout the microstructure. Again, a Cr-rich precipitate was accompanied by a secondary austenite phase, whose composition was roughly 2/3 that of the primary austenite. This depleted phase made the specimen more susceptible to localized corrosive attack, but to a lesser extent than aging at 700°C.

❖ In addition to the Cr-depleted phase that precipitates with thermal aging, some grain boundary Cr depletion was observed as well. The initial drop in E_{rcrev} is a confluence of both of these, though the GBCD is recoverable with time. Reduced corrosion resistance with thermal aging due to the formation of secondary austenite is not recovered with prolonged thermal exposure, and the precipitation of this phase is accompanied by a non-recoverable reduction in localized corrosion resistance as observed with crevice repassivation potential measurements in chloride-containing environments. S32205 aged at 700°C displayed no recovery with prolonged thermal exposure, while aging at 870°C recovered approximately 100 mV of the initial E_{rcrev} drop.

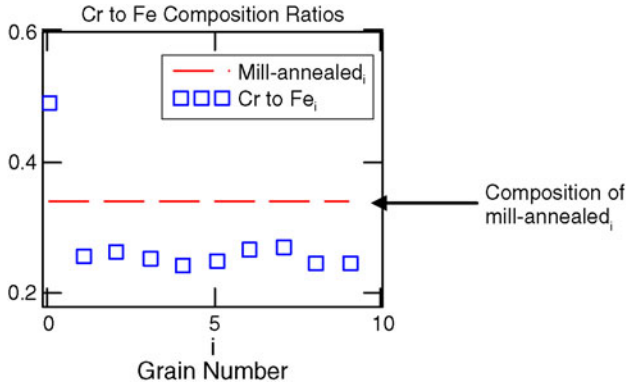

FIGURE 16. *EDS profiles of various selected phases for S32205 after exposure to 870°C for 2 h.*

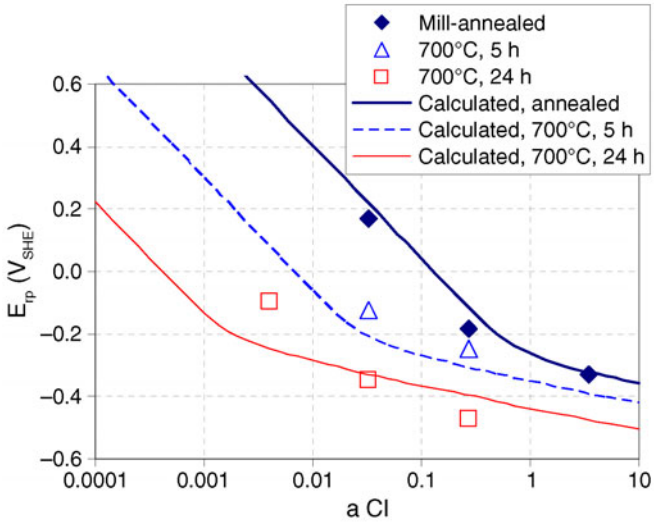

FIGURE 17. *Comparison of experimental (symbols) and predicted (lines) repassivation potentials of Alloy 2205 in a mill-annealed form (diamonds and thick line), after thermal aging at 700°C and 5 h (triangles and dashed line) and after thermal aging at 700°C and 24 h (squares and thin line).*

❖ A previously developed mechanistic model for calculating the repassivation potential of Fe-Ni-Cr-Mo-W-N alloys has been applied to predict E_{rp} of thermally aged alloys on the assumption that the measured E_{rp} values reflect the composition of the phase that is most depleted in Cr (i.e., the secondary austenite). A reasonably good agreement has been obtained, which indicates that the model can be used to predict the repassivation potential of heat-treated as well as annealed samples, as long their microchemical composition is known.

ACKNOWLEDGMENTS

The work reported here has been supported by the U.S. Department of Energy (award number DE-FC36-04GO14043) and co-sponsored by Chevron-Texaco, DuPont, Haynes International, Mitsubishi Chemical, Shell, and Toyo Engineering.

REFERENCES

1. N. Sridhar, L.H. Flasche, J. Kolts, *Mater. Perform.* 21, 12 (1984): p. 50.
2. A.J. Ramirez, J.C. Lippold, S.D. Brandi, *Met. Trans.* 34A (2003): p. 1,575-1,597.
3. N. Sridhar, J. Kolts, *Corrosion* 43, 11 (1987): p. 646.
4. V. Muthupandi, P. Bala Srinivasan, S.K. Seshadri, S. Sundaresan, *Corros. Eng. Sci. Technol.* 38, 4 (2003): p. 303-310.
5. X.-C. Jiang, T. Yoshimura, Y. Ishikawa, T. Shinohara, S. Tsujikawa, *J. Electrochem. Soc.* 139, 4 (1992): p. 1,001-1,008.
6. P. Merino, X.R. Novoa, G. Pena, E. Porto, L. Espada, *Mater. Sci. Technol.* 9, 2 (1993): p. 168-171.
7. K. Ravindranath, S.N. Malhotra, *Corrosion* 50, 4 (1994): p. 318-328.
8. K. Ravindranath, S.N. Malhotra, *Corros. Sci.* 37, 1 (1995): p. 121-132.
9. J.O. Nilsson, *Mater. Sci. Technol.* 11 (1995): p. 276-283.
10. N. Lopez, M. Cid, M. Puiggali, *Corros. Sci.* 41 (1999): p. 1,615-1,631.
11. T. Amadou, A. Ben Rhouma, H. Sidhom, C. Braham, J. Ledion, *Met. Trans.* 31A (2000): p. 2,015-2,026.
12. R.A. Perren, T. Suter, C. Solenthaler, G. Gullo, P.J. Uggowitzer, H. Böhni, M.O. Speidel, *Corros. Sci.* 43 (2001): p. 727-745.
13. C.-J. Park, H.-S. Kwon, *Corros. Sci.* 44 (2002): p. 2,817-2,830.
14. K.L. Weng, T.H. Chen, J.R. Yang, *Bull. Coll. Eng., NTU* 89, 10 (2003): p. 45-61.
15. E. Angelini, B. De Benedetti, F. Rosalbino, *Corros. Sci.* 46 (2004): p. 1,351-1,367.
16. T. Amadou, C. Braham, H. Sidhom, *Metall. Mater. Trans. A* 35A (2004): p. 3,499-3,513.
17. C.J. Park, V.S. Rao, H.S. Kwon, *Corrosion* 61, 1 (2005): p. 76-83.
18. F. Iacoviello, F. Casari, S. Gialanella, *Corros. Sci.* 47 (2005): p. 909-922.
19. G. Tormoen, N. Sridhar, A. Anderko, "Localized Corrosion of Heat-Treated Alloys, Part 1—Repassivation Potential of Alloy 600 as Function of Solution Chemistry and Thermal Aging," *Corros. Eng. Sci. Technol.*, http://www.ingentaconnect.com/content/maney/cest/pre-prints/cst294.
20. Y.-M. Pan, D.S. Dunn, G.A. Cragnolino, N. Sridhar, *Metall. Mater. Trans. A* 31A (2000): p. 1,163-1,173.
21. D.S. Dunn, G.A. Cragnolino, N. Sridhar, "Passive Dissolution and Localized Corrosion of Alloy 22 High-Level Waste Container Weldments," Scientific Basis for Nuclear Waste Management XXIII (Warrendale, PA: Materials Research Society, 2000).
22. A. Anderko, N. Sridhar, D.S. Dunn, *Corros. Sci.* 46 (2004): p. 1,583-1,612.
23. A. Anderko, N. Sridhar, M.A. Jakab, G. Tormoen, *Corros. Sci.* 50 (2008): p. 3,629-3,647.
24. A. Anderko, N. Sridhar, L.T. Yang, S.L. Grise, B.J. Saldanha, M.H. Dorsey, *Corros. Eng., Sci. Technol.* 40, 1 (2005): p. 33-42.